Molecular Biology of the Cell
Vol. 14, 4628–4640, November 2003

# Acroplaxome, an F-Actin–Keratin-containing Plate, Anchors the Acrosome to the Nucleus during Shaping of the Spermatid Head

**Abraham L. Kierszenbaum,* Eugene Rivkin, and Laura L. Tres**

Department of Cell Biology and Anatomical Sciences, The Sophie Davis School of Biomedical Education/The City University of New York Medical School, New York New York 10031

Submitted April 11, 2003; Revised July 10, 2003; Accepted July 14, 2003
Monitoring Editor: Richard J. McIntosh

**Nuclear shaping is a critical event during sperm development as demonstrated by the incidence of male infertility associated with abnormal sperm head shaping. Herein, we demonstrate that mouse and rat spermatids assemble in the subacrosomal space a cytoskeletal scaffold containing F-actin and Sak57, a keratin ortholog. The cytoskeletal plate, designated acroplaxome, anchors the developing acrosome to the nuclear envelope. The acroplaxome consists of a marginal ring containing keratin 5 10-nm-thick filaments and F-actin. The ring is closely associated with the leading edge of the acrosome and to the nuclear envelope during the elongation of the spermatid head. Anchorage of the acroplaxome to the gradually shaping nucleus is not disrupted by hypotonic treatment and brief Triton X-100 extraction. By examining spermiogenesis in the *azh* mutant mouse, characterized by abnormal spermatid/sperm head shaping, we have determined that a deformity of the spermatid nucleus is restricted to the acroplaxome region. These findings lead to the suggestion that the acroplaxome nucleates an F-actin–keratin-containing assembly with the purpose of stabilizing and anchoring the developing acrosome during spermatid nuclear elongation. The acroplaxome may also provide a mechanical planar scaffold modulating external clutching forces generated by a stack of Sertoli cell F-actin–containing hoops encircling the elongating spermatid nucleus.**

## INTRODUCTION

Spermiogenesis is a prolonged cell differentiation process in which the male gamete acquires a propelling flagellum required for delivering the haploid genome to the receptive egg at the time of fertilization. Two major events of spermiogenesis are the development of the acrosome and the shaping and condensation of the future sperm nucleus from a spherical configuration into an elongated structure. The acrosome initiates its development when transporting vesicles derived from the Golgi apparatus fuse to form a single acrosomal sac associated with the nuclear envelope. As the development of the acrosome is in progress, the transient microtubule-containing manchette becomes visible when the spermatid nucleus initiates its elongation. The manchette disassembles upon completion of nuclear elongation and condensation (reviewed by Clermont *et al*., 1993). This developmental correlation has been interpreted as indicative of a possible involvement of the manchette in spermatid nuclear shaping (reviewed by Meistrich, 1993). However, recent experimental evidence supports an intramanchette transport mechanism for the delivery of molecules to the centrosome and developing spermatid tail (reviewed by Kierszenbaum, 2002). Molecular aspects of the possible contribution of the acrosome to spermatid nuclear shaping are beginning to emerge. A lack of acrosome formation in Hrb null mutant mice (Kang-Decker *et al*., 2001) and GOPC-deficient mice (Yao *et al*., 2002) is associated with globozoospermia (round-headed sperm) and infertility. Hrb is associated with the cytosolic surface of proacrosomic transporting vesicles and a lack of Hrb prevents the vesicles from fusing to form the large acrosomal sac. GOPC is localized in the *trans*-Golgi region in round spermatids, and a lack of GOPC precludes vesicle transport from the Golgi apparatus to the acrosomal sac. The developing acrosome embraces the apical one-third of the spermatid nucleus and its configuration gradually follows the shaping of the spermatid nucleus. Because of this relationship, we have considered the possibility of an anchoring mechanism, which prevents the dislocation of the acrosome sac and also modulates extrinsic and/or intrinsic forces operating during nuclear shaping in mammalian spermatids, including human.

Previous work has shown that *s*permatogenic cell/sperm-*a*ssociated *k*eratin of molecular mass *57* kDa (Sak57) provides a cortical scaffold to primary spermatocytes, is present in the core of intercellular bridges connecting members of a spermatocyte cohort (Tres *et al*., 1996), and is associated with microtubules of the manchette before becoming a component of the outer dense fibers surrounding the axoneme of the developing spermatid tail (Tres and Kierszenbaum, 1996). Based on these observations, we have searched for additional sites in which Sak57 may be present during spermiogenesis. Herein, we report the structural characterization of a plate present in the subacrosomal space and linking the developing acrosome to the spermatid nucleus. This plate, which we designate acroplaxome (from the Greek words *akros*, topmost; *platys*, flat; *sōma*, body), consists of F-actin and Sak57 and is bordered by a marginal ring. The marginal ring is made up of Sak57-containing intermediate filaments inserted into a plaque associated with the leading

Article published online ahead of print. Mol. Biol. Cell 10.1091/mbc.E03–04–0226. Article and publication date are available at www.molbiolcell.org/cgi/doi/10.1091/mbc.E03–04–0226.

* Corresponding author. E-mail address: kier@med.cuny.edu.

edge of the inner acrosomal membrane. To identify the molecular nature of Sak57, we have used cDNA cloning. We show that Sak57 is a rat ortholog to human keratin 5 (K5) present in the suprabasal layers of the epidermis. This finding led us to change the designation Sak57 to K5.

## MATERIALS AND METHODS

### *Cloning of Rat Testis K5 (formerly Sak57) cDNA*

Mass spectrometry analysis of high-performance liquid chromatography-fractionated Lys-C–digested Sak57 peptides from rat sperm tail indicated that two fragments displayed homology with the α-helical rod domain (1A and 2A regions) of human, rat, and mouse keratins (for details, see Kierszenbaum *et al*., 1996). Reverse translation of one of the sequences (KAQYEDIAQK) by using mammalian-specific frequency of nucleotide usage resulted in the DNA sequence, which was used to design nested primers (R, TTCTGGGCAATGTCCTC, and T, TCCTCGTACTGGGCCTT). We started cloning of Sak57 cDNA from a rat testis λgt11 cDNA library (BD Biosciences Clontech, Palo Alto, CA) by using nested polymerase chain reaction (PCR) with primers gt11-5′ and R followed by gt11-5′ (GACTCCTGGAGCCCG) and T. Sequencing of an obtained fragment revealed near identity to the mRNA for human keratin 5 (K5). Human K5-specific nested primers spanning the entire coding region were synthesized and used to clone rat testis K5 cDNA.

### *Expression and Analysis of K5 Fusion Protein*

Expression vector pET-Blue2 (Novagen, Madison, WI) was used for directional cloning of a K5 cDNA fragment (encoding amino acids 166–462) into *Sal*I-*Xho*I sites followed by transformation of competent NovaBlue DE3 cells (Novagen). Transformed cells were grown in the presence or absence (control) of 1 mM isopropyl β-D-thiogalactoside (IPTG). Proteins were extracted in extraction buffer (8 M urea, 1% SDS, 10 mM Na phosphate, 0.1 M dithiothreitol) and analyzed by immunoblotting. Purification of K5 fusion protein, which contains $(His)_6$ tail at the carboxy terminus, was carried out using His.Bind Quick 900 cartridge and His.Bind buffer kit (Novagen) according to the manufacturer's protocols. Eluted protein samples were concentrated using a Centricon centrifugal filter (Millipore, Bedford, MA).

### *Construction of a Pachytene cDNA Expression Library*

A rat pachytene cDNA expression library was used to determine the spermatogenic cell-specific expression of K5. Complete details of the construction of the rat pachytene cDNA expression library have been reported previously (Rivkin *et al*., 1997).

### *Affinity Purification and Competition Analysis of Anti-K5 Serum Specificity*

Polyclonal antibodies generated against the peptide KAQYEDIAQK (corresponding to a segment of the 2A region of the α-helical rod domain; Figure 1) and LEGQECRLSGEGVG (corresponding to the beginning of the tail domain) were prepared and characterized as described previously (Kierszenbaum *et al*., 1996). For affinity purification, the antigenic peptide was immobilized to an AminoLink coupling gel column (AminoLink kit; Pierce Chemical, Rockford, IL) according to the manufacturer's protocol. Binding to and elution of specific immunoglobulin from the affinity column was carried out using ImmunoPure Gentle Ag/antibody buffers (Pierce Chemical). The $A_{280}$ protein peak fractions were used for immunocytochemistry and immunoblotting (see below). For competition analysis of antiserum specificity, 3 mg of KAQYEDIAQK peptide or an unrelated peptide was added to 0.1-ml aliquots of affinity-purified anti-K5 serum and incubated overnight at 4°C. These samples were diluted 1:150 and checked for recognition of the K5 fusion protein on immunoblots.

### *Indirect Immunofluorescence, Immunogold Electron Microscopy, and Immunoperoxidase Staining*

The following samples were analyzed: rat and mouse testis, isolated rat spermatogenic cells, and human (plantar) and rat skin (foodtpad and back). Human skin samples were from autopsy specimens, and their use was approved by the Human Subjects Committee (assurance number M-1111-XM-4XM; protocol number H-0021). Seminiferous tubular fragments (identified with a dissecting stereomicroscope as corresponding to stage I-XIV of rat spermatogenesis according to their transillumination pattern; Mochida *et al*., 1999 and references therein for additional details) were placed in a drop of 3.7% paraformaldehyde (electron microscopy grade) in 0.1 M sucrose in phosphate buffer, pH 7.4, on microscope slides coated with Vectabond (Vector Laboratories, Burlingame, CA). After 15-min fixation at room temperatures, spermatogenic cells were gently extruded from the seminiferous tubule by placing a coverglass on top of the preparation. The glass coverslip was removed and used for immunocytochemistry (see below). In some experiments, cells were extracted with 0.5% Triton X-100 in 0.1 M sucrose for 30 s and then fixed for 15 min in paraformaldehyde as indicated above. Cells were immunoreacted with affinity-purified K5 sera alone or double stained with α-tubulin monoclonal antibody (working dilution 1:100; Sigma-Aldrich, St. Louis, MO), followed by anti-rabbit IgG-conjugated with fluorescein isothiocyanate or anti-mouse IgG conjugated with rhodamine (working dilution 1:200; Jackson Immunoresearch Laboratories, West Grove, PA). Specimens were mounted with Vectashield (Vector Laboratories) containing propidium iodide (to detect nucleic acids by a red emission color) or 4,6-diamidino-2-phenylindole (to detect the position of the nucleus by a blue emission color). Acrosomes were labeled with peanut agglutinin (PNA) Alexa Fluor 488 conjugate (Molecular Probes, Eugene, OR) according to the procedure described by Szász *et al.* (2000).

Testes from adult rats (Sprague-Dawley), wild-type mice (C57BL/6J), and *azh* mutant mice (The Jackson Laboratory, Bar Harbor, ME) were used for transmission electron microscopy and immunogold electron microscopy. For transmission electron microscopy, samples were fixed in 2.5% glutaraldehyde in 0.1 M phosphate buffer (pH 6.9) and postfixed in 2% osmium tetroxide in the same buffer, and embedded in a plastic resin according to a standard procedure. For immunogold electron microscopy, samples were fixed in a mixture of 1.5% glutaraldehyde and 3.4% paraformadehyde (electron microscope grade) in 0.1 M phosphate buffer, pH 7.2, embedded in Lowicryl K4M (Polysciences, Warrington, PA), and processed for immunogold microscopy as described previously (Rivkin *et al*., 1997). Anti-K5 polyclonal affinity-purified sera (see above) and β-actin and α-tubulin monoclonal (mouse) antibodies (Sigma-Aldrich) were used at working dilutions of 1:100 in phosphated-buffered saline containing 0.1% Tween 20, 1% bovine serum albumin, and 1% goat serum. Bound antibody was detected by incubating the sample overnight at 4°C with goat anti-rabbit IgG or anti-mouse IgG conjugated with 10-nm gold particles (Amersham Biosciences, Piscataway, NJ), by using a 1:50 working dilution. Sections were stained for 5 min with 5% uranyl acetate in deionized water, and specimens were examined using a JEM-100CX transmission electron microscope operated at an accelerating voltage of 60 kV.

Human and rat skin specimens were fixed in 4% paraformadehyde in 0.1 M phosphate buffer, pH 7.2, for 1 h, embedded in paraffin, and sectioned. Sections were immunoreacted with anti-K5 serum (working dilution: 1:100 for immunofluorescence and 1:3000 for immunoperoxidase) and processed using standard procedures. A commercial affinity-purified polyclonal antiserum to mouse K5 (working dilution 1:100; Covance, Richmond, CA) was used as an additional control for antibody specificity (our unpublished data).

## RESULTS

### *cDNA Cloning Shows That Rat Testis Sak57 Is an Ortholog of Human and Mouse Keratin 5*

cDNA cloning was carried out as described in MATERIALS AND METHODS. An analysis of the deduced amino acid sequence of rat testis Sak57 shows an overall 89% homology with human K5 (Figure 1, conservative substitutions are also indicated). The rod domain is the most conserved segment of K5 with 98% homology in both human and mouse (our unpublished data) K5. It has a typical length for keratins (304 amino acids) with well-conserved start and end sequences (IKTLNNKFASF and EIATYRKLLEG, respectively). The head and tail domains of K5 have significantly lower homology. In particular, the head domain has 88% homology with both human and mouse K5, whereas the tail domain has 69 and 50% homology with human and mouse K5, respectively. These lower homologies are estimates because they were obtained by introducing gaps in the sequences. Reverse transcription-PCR analysis by using rat testis total RNA and a rat pachytene spermatocyte cDNA library demonstrates the expression of K5 transcripts during spermatogenesis (Figure 2A).

The subdomain 2A contains the amino acid sequence KAQYEDIANR, which is identical to that previously found by others by partial amino acid sequencing of rat epidermal K5 (see Figure 2 in Kierszenbaum *et al*., 1996, and references therein), but differs by two carboxyl terminal amino acids from the one obtained by mass spectrometry analysis of purified Sak57 (KAQYEDIAQK). This peptide was used to raise a polyclonal anti-K5 serum and for affinity purification (Kierszenbaum *et al*., 1996). To verify that this antibody actually recognizes K5 pro-


**Figure 1.** Comparison of rat testis Sak57 (now designated K5) and human K5 amino acid sequences. The symbol + denotes conservative substitutions. Gaps were introduced to maximize homology. The diagram (not to scale) at the bottom indicates the head, rod, and tail domains of K5, as well as the subdomains and linkers of the rod domain. The corresponding amino acid sequences of the domains, subdomains, and linkers are indicated for both rat testis K5 (Sak57) and human K5 (hK5). The conserved sequences KAQYEDIANR in the 2A subdomain and LEGQECRLSGEGVG in the 2B-tail domain junction are indicated in yellow. GenBank accession number AY342389.

tein, a cDNA fragment containing this sequence was cloned into the expression vector pBlue-2 and the fusion protein was expressed in *Escherichia coli*. Figure 2B demonstrates that anti-K5 antibody recognizes the fusion protein produced upon induction by IPTG. The specificity of anti-K5 serum was verified by competition experiments (Figure 2C). The KAQYEDIAQK peptide completely blocked recognition of the fusion protein by the affinity-purified K5 antibody. In contrast, an unrelated peptide had no effect.

### *Anti-K5 Antibodies Detect Identical Antigens in Human and Rat Epidermis*

We have used affinity-purified polyclonal antibodies generated in rabbit against the peptides KAQYEDIAQK (corre-

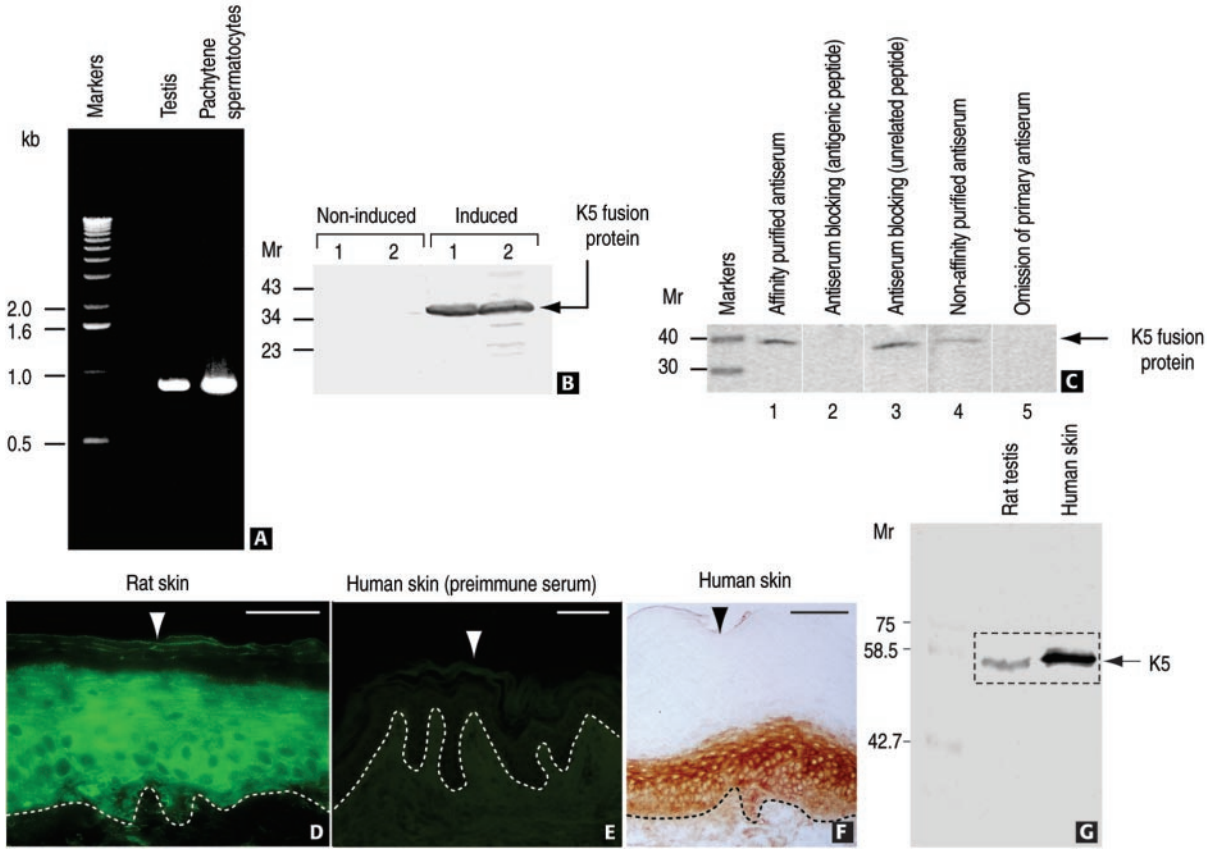


**Figure 2.** Expression and localization of K5 in rat testis and skin using affinity purified antibodies. (A) Gene expression of K5 in rat testis and pachytene spermatocytes demonstrated by PCR with total rat testis RNA and a rat pachytene spermatocyte cDNA library. (B) A fusion protein of the cloned rat testis K5 cDNA (see MATERIALS AND METHODS) is recognized by anti-K5 sera. Two independent clones (1 and 2) under IPTG-inducing and noninducing conditions are shown. (C) Recognition of His-purified fusion protein by affinity-purified anti-K5 serum is blocked by fusion K5 peptide (lane 2). In contrast, an unrelated peptide does not affect antigen recognition (lane 3). Lanes 1 and 4, affinity-purified and not purified anti-K5 sera; lane 5, control (secondary alkaline phosphatase-conjugated anti-rabbit serum). Numbers at the left indicate the position of molecular mass ($M_r$) markers. (D–F) Immunohistochemical localization of K5 in rat (D, immunofluorescence) and human epidermis (F, immunoperoxidase) by using anti-rat K5 serum (D) and anti-mouse K5 serum (F). (E) Negative control (preimmune serum). The dotted line indicates the epidermis-dermis boundary. The arrowhead denotes the outer layer of the epidermis. Bars (D–F), 100 $\mu$m. (G) Immunoblot showing the equivalent molecular mass of rat testis and human skin (epidermis) K5.

sponding to a segment of the 2A region of the $\alpha$-helical rod domain) and LEGQECRLSGEGVG (corresponding to the beginning of the tail domain) to determine specific immunoreactive sites in rat and human epidermis. Figure 2, D and F, demonstrate the localization of K5 immunoreactive sites in the suprabasal layer of the rat epidermis (Figure 2D; indirect immunofluorescence) and human epidermis (Figure 2F; immunoperoxidase), where K5 is known to coexist with keratin 14. Specific immunoreactivity was not detected in human epidermis incubated with preimmune serum (Figure 2E; negative control). Immunoblotting experiments, using testis and human skin lysates, demonstrate that the K5 antiserum detects a 57-kDa immunoreactive protein band in both rat testis and human epidermis samples (Figure 2G). A similar immunoblotting experiment, using anti-mouse K5 antibody, yielded similar results (our unpublished data).

### *K5 and β-Actin Antigenic Sites Coexist in the Acrosomal Region of Developing Rat Spermatids*

With these results, indicating a distinct immunoreactive homology of rat testis Sak57 and rat and human epidermal K5, we focused our search of K5 immunoreactive sites in whole rat spermatids collected from spermatogenic stage-specific seminiferous tubules (Figure 3). A mild hypotonic treatment with 0.1 M sucrose (selected panels in Figure 3) and brief Triton X-100 extraction (Figure 4) were used to determine whether the K5-containing acroplaxome remained firmly attached to the spermatid nucleus. As the acrosome extends caudally along the spermatid nucleus and the manchette initiates its development (step 8 of spermiogenesis), a conspicuous K5-immunoreactive ring coinciding with the boundary of the acrosome was visualized (Figure 3, A–E). The developing manchettte, flanking the spermatid nucleus, displayed both tubulin and K5 immunoreactivity. During step 12, both the fully developed microtubular manchette and the acrosome, descending along the elongating spermatid nucleus, are K5 immunoreactive (Figure 3, F and G). The association of K5 with microtubules of the manchette was reported previously (Tres and Kierszenbaum, 1996). During step 17, when the manchette has fully disassembled, K5 immunoreactive sites occupy a caudal nuclear distribution (Figure 3, H–K). A $\beta$-actin immunoreactive ring was ob-

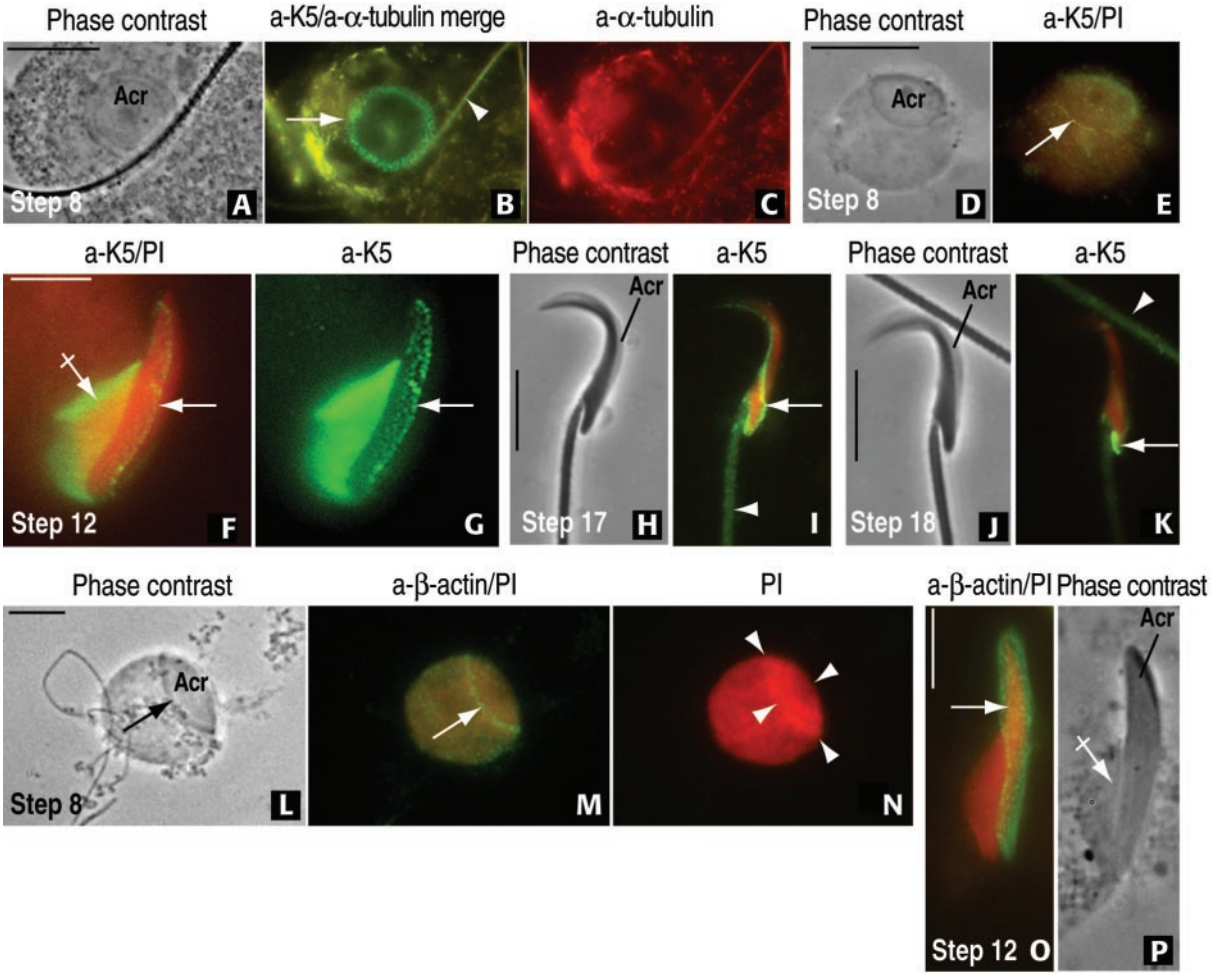


**Figure 3.** Development of the acroplaxome during rat spermiogenesis by using antibodies to K5 and β-actin. (A–C) A step 8 spermatid displays a top view of the acrosome (acr, A). The 1-μm-wide marginal ring of the acroplaxome (arrow) and an overlapping spermatid tail (arrowhead) are K5 immunoreactive (B). α-Tubulin–stained microtubules of the manchette are seen eccentric to the acroplaxome in C. (D and E) Step 8 spermatid subjected to hypotonic treatment to remove the cytoplasm and stained with anti-K5 serum and propidium iodide (PI). The K5-immunoreacted acroplaxome (arrow) remains attached to the spermatid nucleus. (F and G) Step 12 spermatid displaying the K5 immunoreactive manchette (crossed arrow) and acroplaxome (arrow) attached to the elongating PI-stained spermatid nucleus. (H and I) Step 17 spermatid. The K5 stained component of the acroplaxome occupies a caudal site (arrow), and the spermatid tail (arrowhead) displays similar immunoreactivity. (J and K) Step 18 spermatid showing a more caudal localization of K5 immunoreactivity. An immunoreactive spermatid tail (arrowhead) is seen in the field. (L–N) Step 8 spermatid is devoid of cytoplasm after hypotonic treatment but retains the acrosome (acr, arrow). The marginal ring of the acroplaxome (arrow) is β-actin immunoreactive (compare with E). (N) Strong and uniform cap-like PI nuclear staining at the acroplaxome site (denoted by arrowheads). (O and P) Step 12 spermatid. The arrow points to the β-actin immunoreacted acroplaxome. The manchette (crossed arrow in P) seems essentially nonimmunoreactive by immunofluorescence (compared with F and G). Bars, 5 μm.

served during step 8 of spermiogenesis at the boundary of the acrosome (Figure 3M; compare with Figure 3, B and E, showing similar K5 localization sites). During step 12, both K5 and β-actin immunoreactive sites coexisted in the acroplaxome. A difference with K5 is the less obvious β-actin immunofluorescent localization in the manchette (compare Figure 3, F and G, and O and P). A strong propidium iodide nuclear-stained region correlates with the cap-like projection of the acrosome (Figure 3N). We concluded from these observations that a K5/β-actin-containing acroplaxome is present at the acrosome-nuclear boundary and that the acroplaxome marginal ring is better visualized in round spermatids when the orientation is either frontal or slightly lateral.

Figure 4, A–D (steps 4 and 5 of spermiogenesis), and E–H (step 6) demonstrate that a combination of sucrose hypotonic treatment and a brief Triton X-100 extraction step before fixation removes most of spermatid cytoplasm, leaving relatively undisturbed the acrosomal vesicle and associated Golgi apparatus. A shallow nuclear indentation accommodates the acrosome. The boundary of shallow indentation displays a distinct propidium iodide-stained nuclear band (Figure 4G), suggesting a different degree of chromatin condensation at this site. To determine whether the marginal ring was not due to a peripheral accumulation of acrosomal enzymes, specimens were stained with PNA conjugated with Alexa Fluor 488 to selectively label the acrosome (Szász *et al*., 2000). Figure 4, I–L, demonstrates that the entire acro-

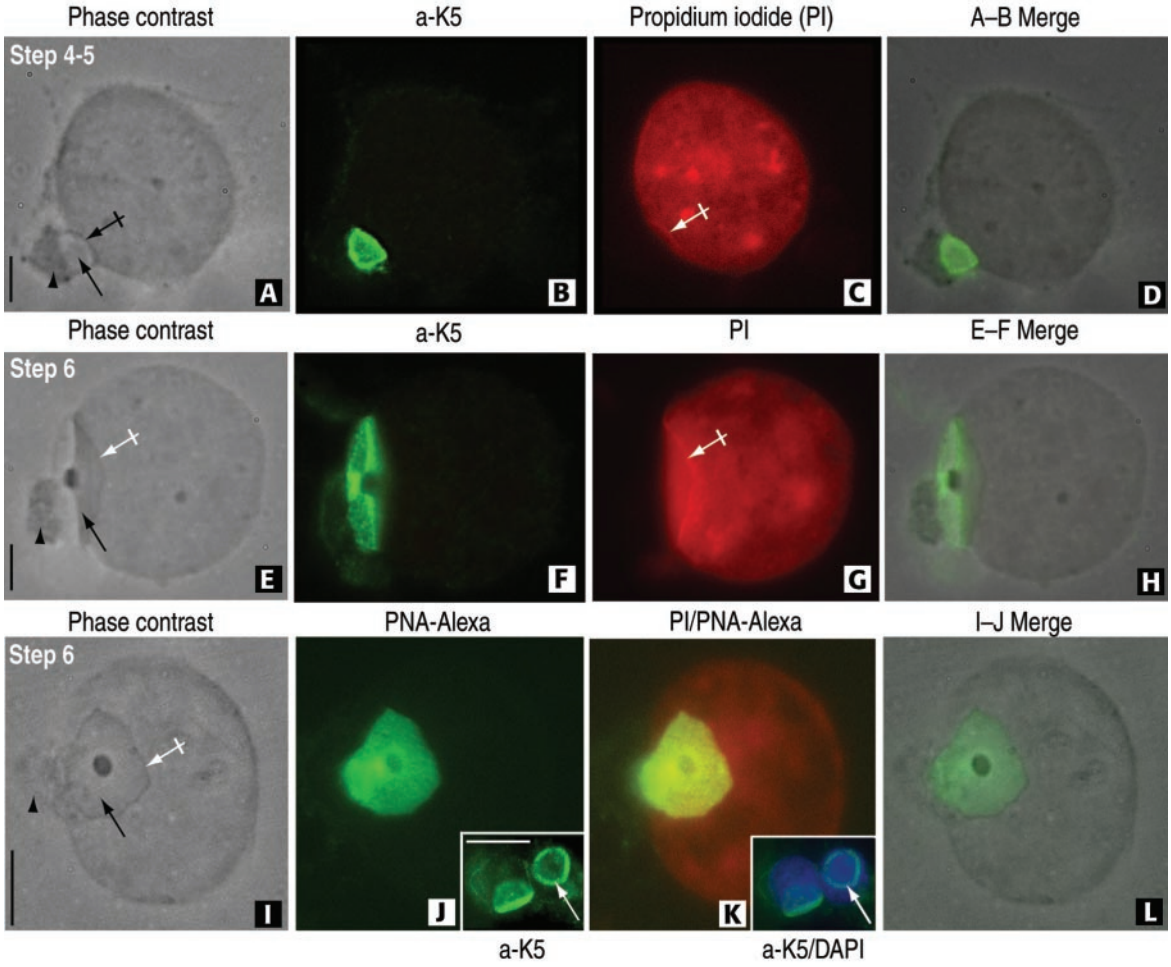


**Figure 4.** The attachment of the rat spermatid acroplaxome to the nuclear envelope is not disrupted by Triton X-100 extraction before fixation. (A–D) A step 4 to 5 spermatid displays in A its acrosome (arrow) lodged in a shallow depression of the nucleus (crossed arrow). The Golgi apparatus (arrowhead) remains attached to the acrosome. The K5-immunoreactive acroplaxome is shown in B. (C) A linear profile of propidium iodide-stained nuclear material is seen along the shallow depression (crossed arrow). (E–H) Step 6 spermatid displays the same features observed in the A–D sequence except that the linear propidium iodide stained nuclear material is more extensive and matching the length of the acroplaxome. (I–L) Step 6 spermatid showing a frontal view of the acrosome (arrow) surrounded by a dense edge (crossed arrow) and associated Golgi apparatus (arrowhead). (J) PNA-Alexa Fluor 488 conjugate uniformly stains the acrosome and the proximal components of the Golgi apparatus. In contrast, the insets in panels J and K show the marginal ring of the K5-stained acroplaxome (inset in J) overlapping the 4,6-diamidino-2-phenylindole-stained nuclei (inset in K) not visualized after PNA-Alexa Fluor 488 staining. Bars, 3 $\mu$m.

some, including the marginal region of a step 6 spermatid, stains evenly, in contrast with the ring-like distribution of K5 seen in the same developmental step (Figure 4, J and K, inset).

### *The Marginal Ring of the Acroplaxome Contains Bundles of K5-Immunoreactive Intermediate Filaments Associated with F-Actin*

Indirect immunofluorescence suggested that $\beta$-actin and K5-containing elements were evenly distributed along the acroplaxome and clustered at the marginal ring. The structure of the ring was analyzed further by electron microscopy. Parallel aligned and obliquely oriented bundles of filaments with respect the nucleus can be visualized at the leading edges of the acroplaxome (rat spermatid, Figure 5A). In a sagittal view (mouse spermatid; Figure 5B), the marginal ring of the acroplaxome displays cross-sectioned 10-nm-thick filaments attached to a dense plaque bound to the inner acrosome membrane. F-Actin microfilaments (7 nm in thickness) in the Sertoli cell ectoplasmic region and microtubules of the manchette (25 nm in width) in the same microscopic field provide support to the different thickness of the intermediate filaments. The K5 immunoreactive filaments can also be visualized by immunofluorescence at the expected position and angular orientation (Figure 5, C and D).

Immunogold electron microscopy demonstrates the presence of K5 immunoreactivity in the subacrosomal region where the acroplaxome and marginal ring are located (Figure 6, A and B). Similar localization sites are seen for $\beta$-actin (Figure 6C). Scattered $\beta$-actin is also seen in the manchette in agreement with a previous report (Mochida *et al*., 1998) We concluded from these combined immunofluorescence and immunogold electron microscopy observations that F-actin and K5 coexist in the acroplaxome and that these two cytoskeletal components are concentrated at the marginal re-

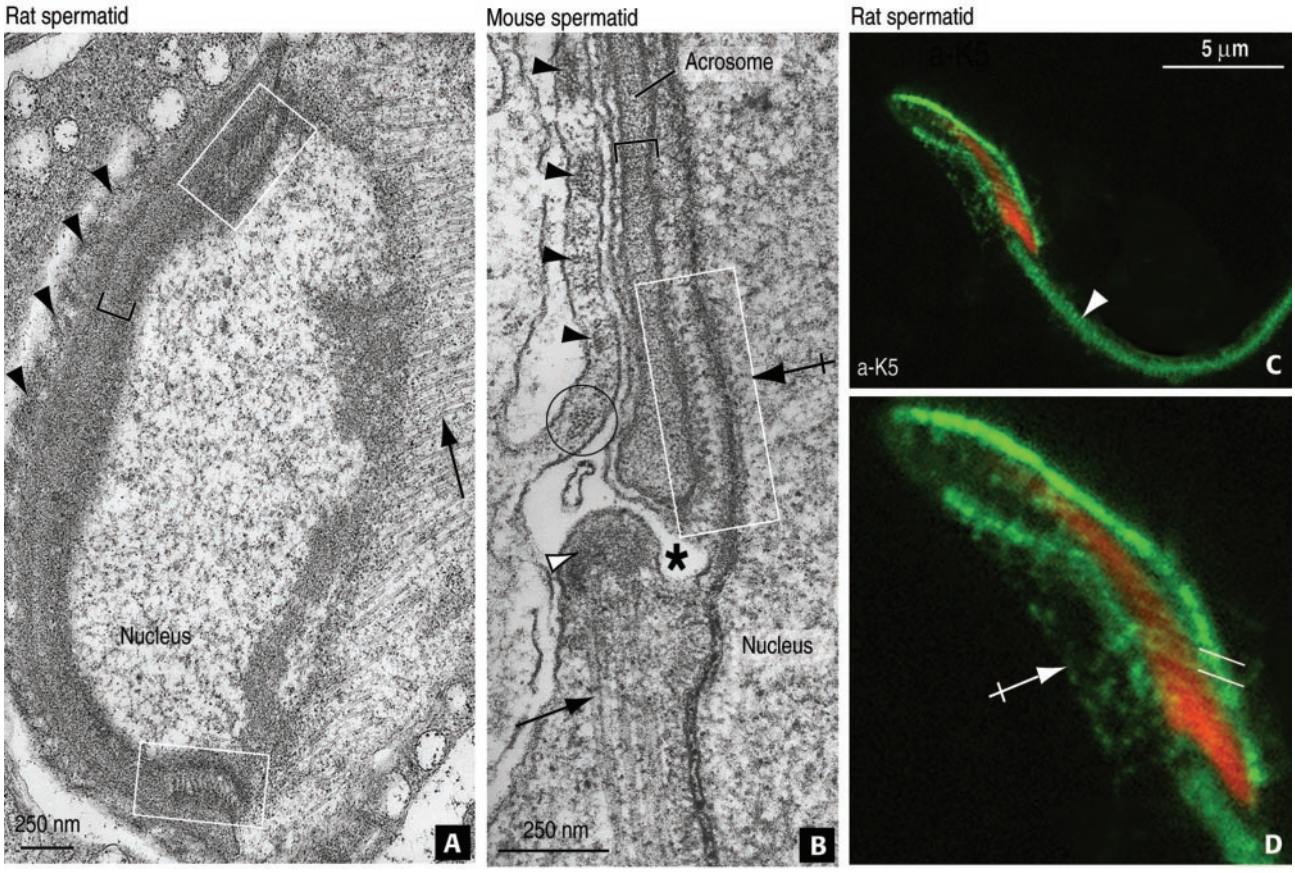


**Figure 5.** Fine structure of the rat and mouse acroplaxome and K5 and β-actin localization sites detected by immunogold electron microscopy. (A) Step 9 rat spermatid sectioned at oblique angle demonstrates the central portion of the acroplaxome (bracket) flanked by the marginal ring in which intermediate filaments bundles are visualized (boxes). The manchette (arrow) and adjacent Sertoli cell ectoplasmic F-actin bundles (arrowheads) are seen. (B) Sagittal view of the acroplaxome marginal ring of a step 10 mouse spermatid. The rectangular box denotes a bundle of intermediate filaments attached to a dense plaque associated with the inner acrosome membrane. The thickness of the intermediate filaments (10 nm) can be compared with adjacent microfilaments (7 nm, circle) of the ectoplasmic Sertoli cell region where actin bundles are located (black arrowheads) and microtubules of the manchette (25 nm, arrow) inserted in the perinuclear ring (white arrowhead). The asterisk indicates a groove separating the acroplaxome-acrosome leading edge from the perinuclear ring of the manchette. (C and D) Step 12 rat spermatid immunoreacted with anti-K5 affinity-purified serum showing the staining of the acroplaxome, the manchette (crossed arrow), and spermatid tail (arrow). The parallel lines in D indicate the angular orientation of the intermediate filaments of the acroplaxome margin.

gion of this subacrosomal plaque. Figure 7 presents a summary of the relevant aspects of acroplaxome development in rat spermatids within a graphic and descriptive context.

### *The Acroplaxome and Manchette in Abnormally Shaped Spermatid Nuclei of the azh Mutant Mouse*

Mutant mouse models in which spermatid nuclear shaping is defective can provide clues concerning the significance of the acroplaxome in the elongation of the spermatid nucleus. Previous studies have shown that, in the *azh* mutant mouse, a relative number of spermatids display abnormally shaped nuclei, sperm have coiled tails (Mochida *et al*., 1999; Akutsu *et al*., 2001), and the fertility rate is significantly reduced (reviewed by Meistrich, 1993). Figure 8A illustrates an elongating spermatid in which the acroplaxome-containing region is particularly indented. A similar feature was observed in mouse offspring produced from normal mouse oocytes injected with sperm heads from the *azh* mutant (see Figure 4, B and C, in Akutsu *et al*., 2001). An additional deformity during the nuclear shaping of the *azh* spermatid mutant is the presence of a nuclear constriction at the site where the perinuclear ring of the manchette is located (Figure 8B). These observations suggested that stress forces acting upon and/or generated by the acroplaxome were unbalanced and prone to generate focal deformities.

## DISCUSSION

We report herein structural details and the partial molecular characterization of the acroplaxome, an attachment plate present in the subacrosomal space of mammalian spermatids (including mouse, rat, and human) and linking the inner acrosomal membrane to the nuclear envelope. The acroplaxome contains F-actin and K5 and presumably other actin-associated proteins and motor proteins, which may be responsible for tethering the primary proacrosomal vesicle during the early stages of acrosomal biogenesis. A specific feature of the acroplaxome is its marginal ring housed in a shallow circular indentation of the spermatid nucleus. An attribute of the marginal ring is a conspicuous bundle of

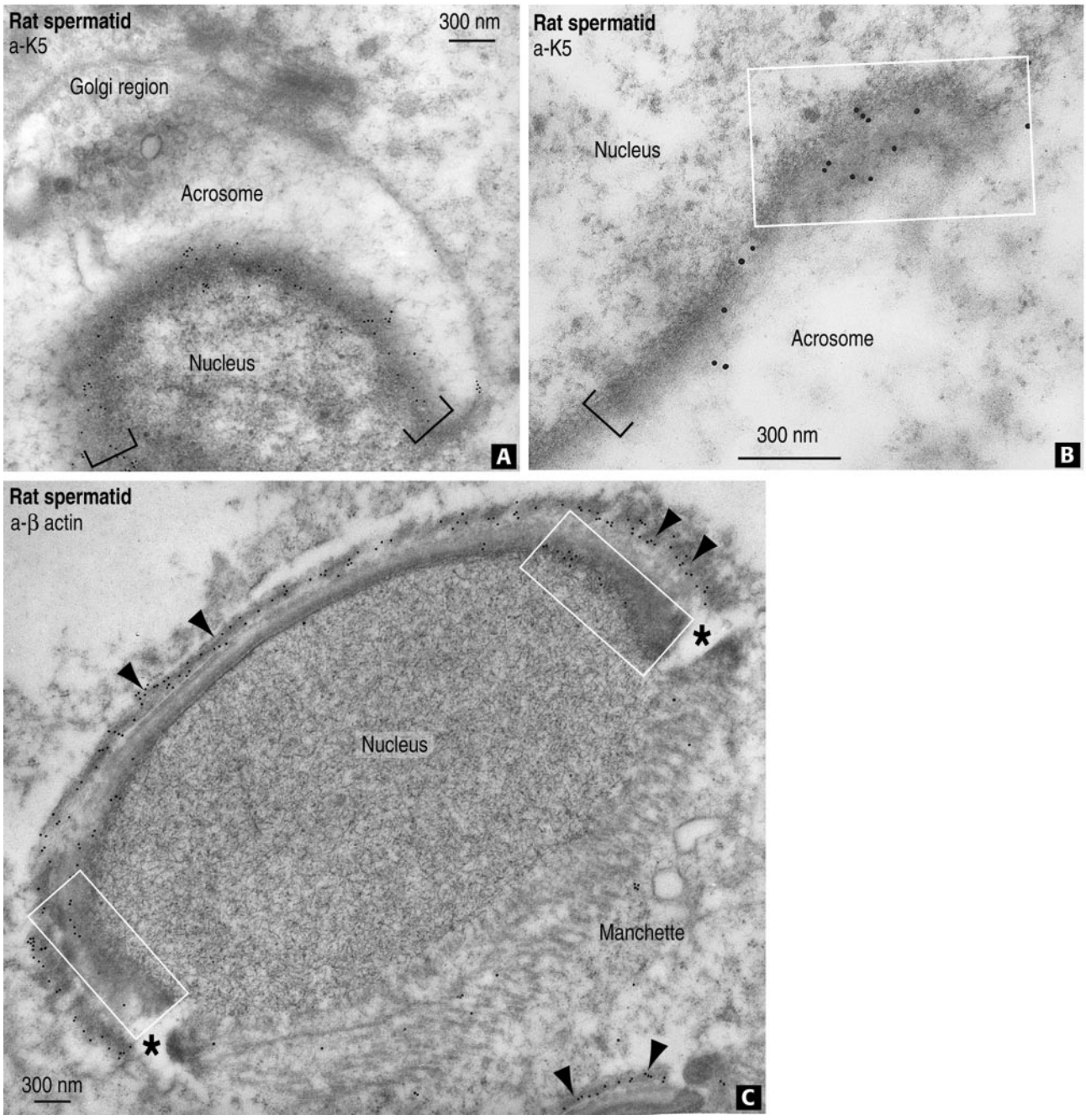


**Figure 6.** Immunogold localization of K5 and β-actin in rat spermatids. (A) Gold particles representing K5 antigenic sites are seen along the rat spermatid acroplaxome (indicated by the brackets) shown in an tangential orientation. (B) K5 immunoreactive sites at the rat spermatid acroplaxome margin (rectangular box) and its adjacent region (bracket). (C) Strong β-actin immunoreactivity is detected along the rat spermatid acroplaxome, the flanking zones representing the marginal ring (rectangular boxes), and F-actin–containing bundles of the Sertoli cell ectoplasm (arrowheads). Diffuse β-actin staining is seen in the manchette region. The asterisks indicate the groove at the acroplaxome/acrosome-manchette interface.

10-nm-thick intermediate filaments attached to the dense plaque associated with the inner acrosomal membrane. The finding of intermediate filaments in the acroplaxome is not surprising. In fact, intermediate filament-like structures in the subacrosomal space were reported previously (Russell *et al*., 1986). However, neither their biochemical nature nor regular organization at the marginal ring of the acroplaxome was described. Opposite to the intermediate filament–plaque complex is another thin plaque spanning across a shallow indentation in the spermatid nuclear envelope and linked to a nuclear lamina (see Figure 9 for a summary diagram). The subacroplaxome position of the nuclear lamina correlates with the propidium iodide dense chromatin staining seen in Figure 4G. The band-like edge of the chromatin density correlates with the collar-like arrangement of the plaque housing the marginal ring of the acroplaxome.

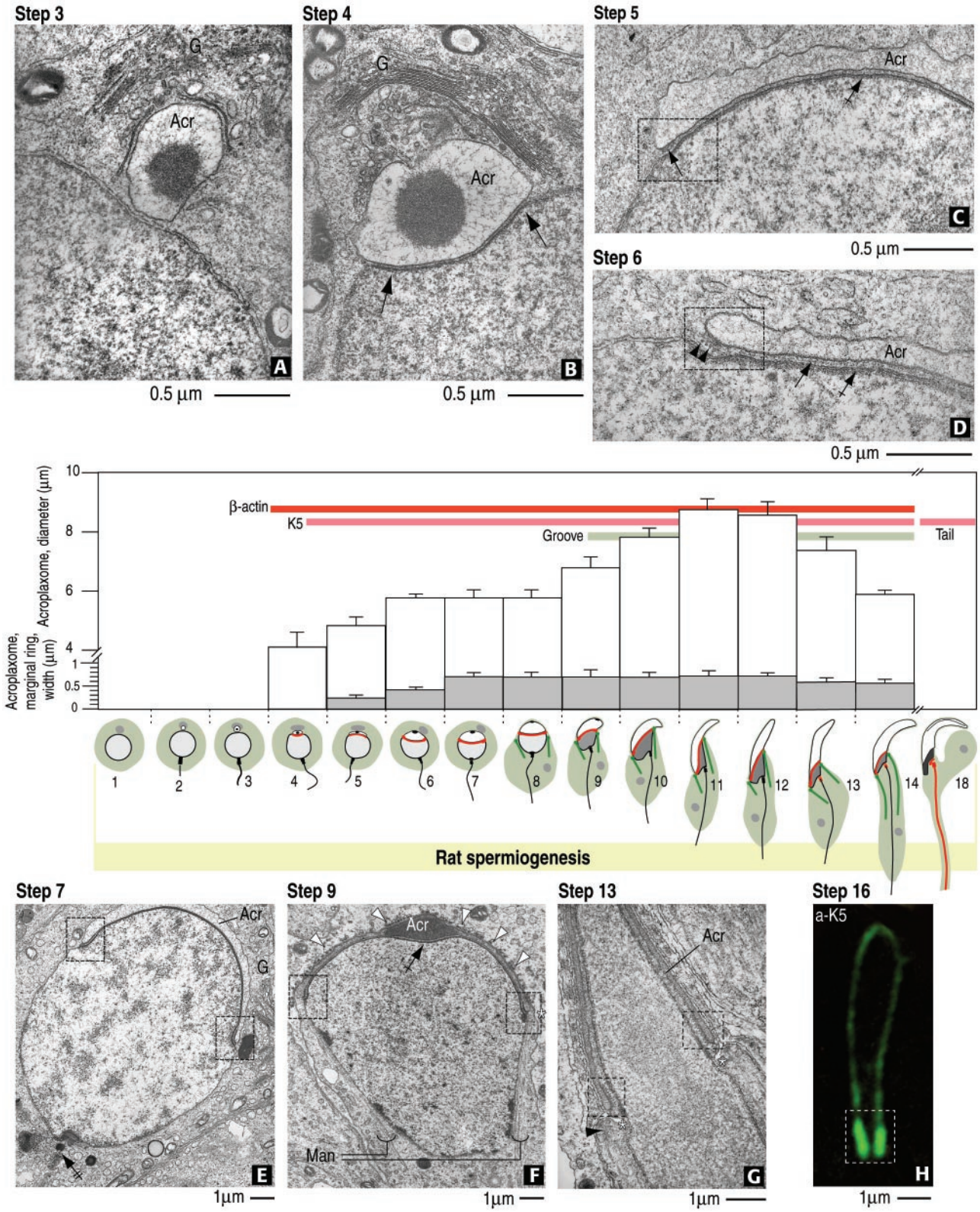


**Figure 7.** Summary diagram of the relevant steps of acroplaxome development during rat spermiogenesis and the emergence of β-actin, K5 immunoreactivity, and the groove. (A) Step 3. A Golgi-derived (G) acrosome vesicle (Acr) contacts the nuclear envelope but the acroplaxome is not visualized. (B) Step 4. The acrosome vesicle is lodged in a shallow depression of the nucleus (arrows) where the density of the acroplaxome is seen. (C) Step 5. The inner acrosomal membrane-associated plaque (dashed box) at the leading edge of the acroplaxome (arrow) is detected. (D) Step 6. An intermediate filament bundle (arrowheads) is seen attached to the acrosome (Acr)-linked plaque. The density of the acroplaxome is indicated by the arrows. (E) Step 7. Shallow indentations at the margins of the acroplaxome (dashed boxes) are

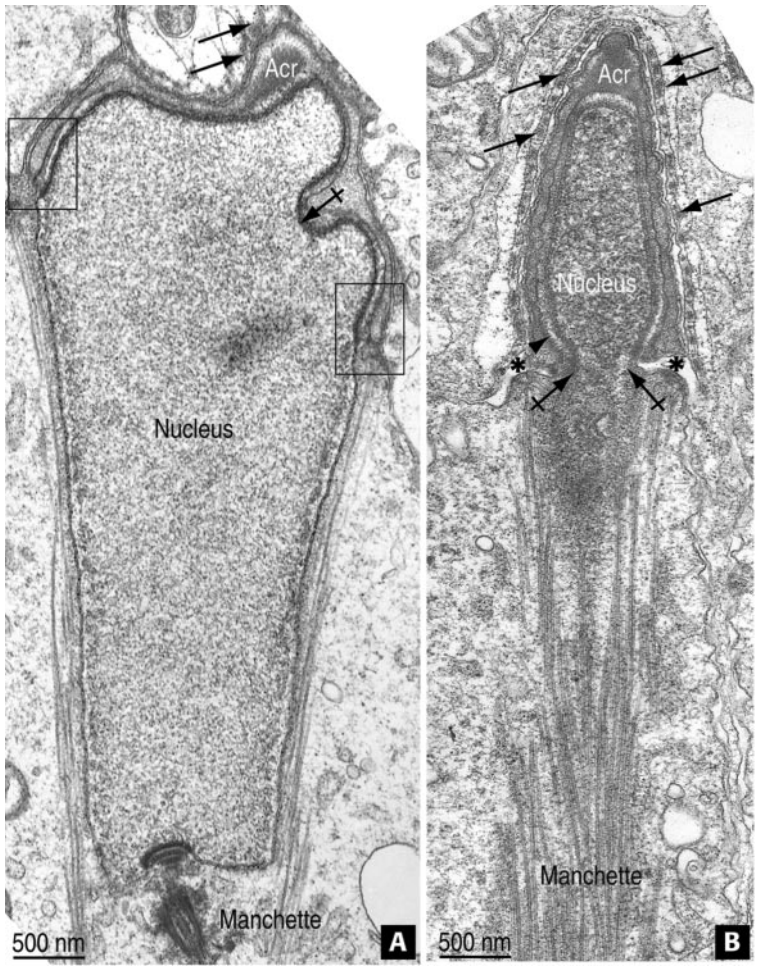


**Figure 8.** The acroplaxome and perinuclear ring of the manchette in *azh* mutant mouse spermatids. (A) The acroplaxome corresponds to the top folded portion of the elongating spermatid nucleus capped by the acrosomal sac (Acr). The boxes indicate the marginal ring; the crossed arrow indicates a deep infolding of the acroplaxome. The arrows point to actin filament bundles and associated endoplasmic reticulum cisternae in the Sertoli cell ectoplasm. The microtubules of the manchette are present. (B) The apical pole of the condensing and elongating nucleus of a spermatid is covered by the Acr. Ectoplasmic actin bundles in the Sertoli cell cytoplasm are indicated by the arrows. The arrowhead points to the marginal ring region of the acroplaxome. The groove belt region is denoted by asterisks. The crossed arrows indicate a nuclear constriction at the juncture of the groove and perinuclear ring of the manchette.

The marginal ring and associated plaques are reminiscent of the zonula adherens belt conjoining the plasma membranes of adjacent epithelial cells. During spermiogenesis, the F-actin/K5-containing marginal ring trails the descending leading edge of the acrosomal sac and then seems to disassemble when nuclear elongation reaches completion (Figure 7). This steady association implies that the acroplaxome is expected to adjust its diameter and shape without compromising the relationship of the marginal ring with both the descending acrosomal edge and the elongating spermatid nucleus. In this regard, the insertion plaques, whose molecular components are presently unknown, may play a pivotal role in stabilizing the position of the acroplaxome. Because gentle hypotonic and mild Triton X-100 treatment cannot dislodge the acrosome–acroplaxome complex from its nuclear attachment site, we postulate that the acroplaxome secures the acrosome at the corresponding nuclear pole during the elongation of the spermatid head. Several observations in mouse mutants with sperm head abnormalities determined by deficient acrosome development (Hrb mutant, Kang-Decker *et al*., 2001; GOPC mutant, Yao *et al*., 2002) make this an attractive hypothesis. As a corollary, a defect in acrosome biogenesis is likely to hamper the assembly and function of the acroplaxome in nuclear shaping.

There are two aspects of this work that merit further discussion. First, the expression of classical keratins and outer dense fibers (Odfs) during spermatogenesis and spermiogenesis in particular. Second, the potential mechanical contribution of the acroplaxome to the nuclear shaping of the male gamete. Both nucleotide sequence analysis and deduced amino acid sequence demonstrate that testicular K5 has a 89% amino acid homology with K5, a type II keratin

**Figure 7 (cont).** detected when the acrosome (Acr) initiates its caudal descent. Neither the groove nor the manchette are present. The double-crossed arrow points to the assembling head-to-tail coupling apparatus. (F) Step 9. Elongation of the spermatid nucleus occurs as the marginal regions of the acrosome and acroplaxome (dashed boxes) continue their descent. The manchette (Man) is now assembled. (G) Step 13. A groove belt (asterisks) develops between the acrosome/acroplaxome leading edge (dashed boxes) and the perinuclear ring of the manchette (arrowhead). (H) Step 16. The leading marginal portion of the acroplaxome displays intense K5 immunoreactivity (dashed box). In the bar graph, the white boxes indicate the average diameter (micrometers) of the acroplaxome, and the gray boxes indicate the width (micrometers) of the acroplaxome marginal ring. In the illustrations representing rat spermiogenic steps, the gray region indicates the Golgi apparatus, the white space corresponds to the acrosome vesicle and acrosome, and the red line denotes the position of the acroplaxome. The manchette is indicated by two green lines extending into the cytoplasm. In step 18, the centrosome region (continuous with a long red line representing the developing tail) displays K5 immunoreactivity. The developmental appearance of $\beta$-actin and K5 immunoreactivity and the groove are indicated by the corresponding color bars.

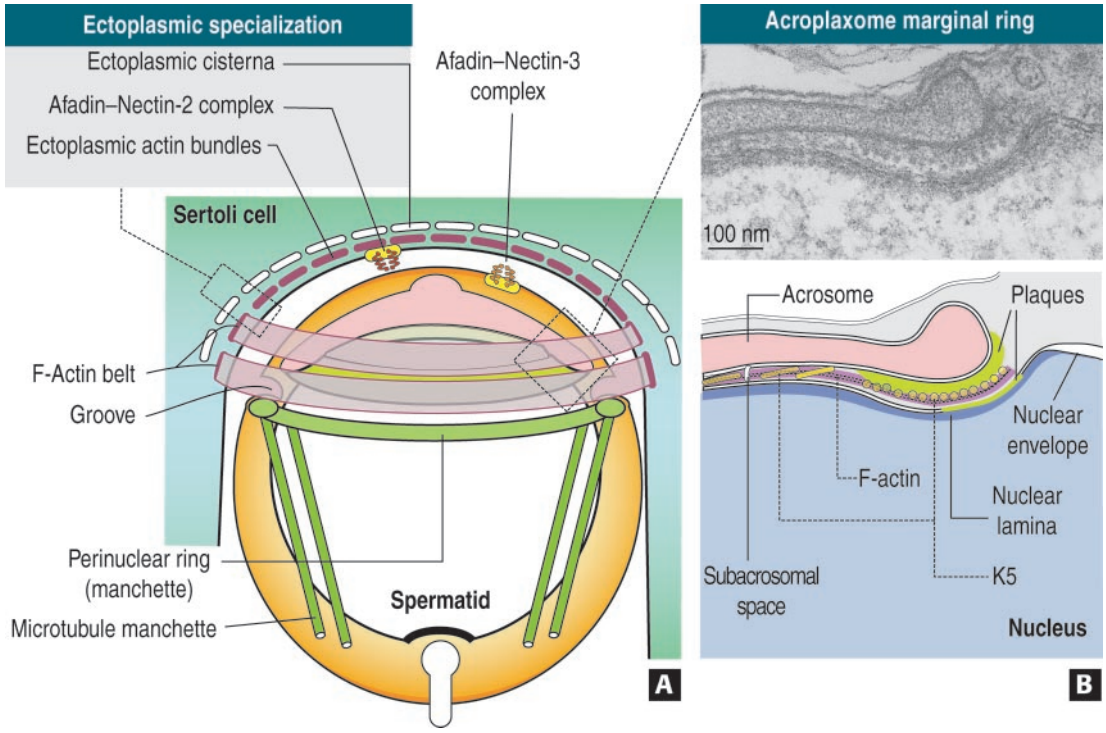


**Figure 9.** Proposed mechanism of spermatid nuclear elongation in rodents. (A) The apical pole of a round spermatid is encircled by parallel F-actin hoops originated in the ectoplasmic region of a Sertoli cell. In the ectoplasmic margin, actin-containing bundles are associated with both ectoplasmic cisternae and afadin–nectin-2 complexes (Takai and Nakanishi, 2003). The extracellular domain of nectin-2 extends into the extracellular space where it may interact with the extracellular domain of nectin-3, bound to afadin at the spermatid cortical cytoplasmic region. This heterotypic junction seems to stabilize the Sertoli cell–spermatid relationship. The acrosome–acroplaxome complex is separated from the perinuclear ring of the manchette and inserted microtubules of the mantle by a belt-arranged groove. The actin belt presumably exerts a gentle and gradual clutching force probably transmitted to the acroplaxome anchored to the elongating spermatid nucleus. The perinuclear ring of the manchette reduces its diameter to adjust to the reducing diameter of the elongating and condensing spermatid nucleus. Diagram not to scale. (B) The acroplaxome marginal ring (seen in a cross sectional orientation in the electron micrograph and the corresponding diagram below) is lodged in a subacrosomal space defined by the leading edge of the acrosomal sac and a shallow indentation in the nucleus, which harbors a narrow dense plaque. The subacrosomal marginal space is occupied by F-actin, K5-containing intermediate filament bundles, and presumably motor proteins (our unpublished data). The K5 filament bundle is attached to the dense acrosomal plaque, whose constituents are presently unknown. A nuclear lamina, also of unknown composition, extends along the closely apposed membranes of the spermatid nuclear envelope.

abundant in the basal layers of the epidermis (Fuchs, 1996). K5 forms a cortical cytoplasmic shell in primary spermatocytes, is present in the centrosomal region during late male meiotic prophase I, is a component of the cytoplamic bridges conjoining cohorts of spermatocytes (Tres *et al*., 1996), and is associated first with the manchette and later with the Odfs and fibrous sheath of the developing tail during rat (Kierszenbaum *et al*., 1996; Tres and Kierszenbaum, 1996) and mouse spermiogenesis (Akutsu *et al*., 2001). A role of K5 in spermatogenesis is supported by the occurrence of significant apoptosis during meiotic prophase and spermatid nuclear and tail abnormalities in selected seminiferous tubules of K5+/− mutant mice (testis samples provided by Thomas M. Magin and Lu Hong, University of Bonn, Germany). Spermiogenesis in K5 null mice cannot be evaluated because they exhibit neonatal lethality (Peters *et al*., 2001). Another keratin, K9, is one of the components of the perinuclear ring of the manchette (Mochida *et al*., 2000). K9 is a unique keratin because its expression is predominant in the epidermis of palm and sole (human) and footpad of rodents and other species. K9 and K5 are examples of type I keratin (which includes K9 to K20) and type II keratin (which includes K1 to K8), respectively, thus far detected during spermatogenesis. At least one member of each family of keratins is required to form heterodimeric intermediate filament proteins. In fact, we have found that keratins 14 and 2e, the common partners of K5 and K9, respectively, are also expressed in testis (our unpublished data).

It is significant to point out that Odfs are cytoskeletal proteins that are heavily disulfide-linked, contain repeats of the Cys-X-Promotif, and surround the axoneme of the sperm tail (Calvin and Bedford, 1971; Olson and Sammons, 1980; Vera *et al*., 1984; Oko, 1988). Three Odfs have been so far reported: Odf1 (27 kDa, van der Hoorn *et al*., 1990; Burfeind and Hoyer-Fender, 1991), Odf2 (84 kDa, Brohmann *et al*., 1997), and Odf3 (110 kDa, Petersen *et al*., 2002). An Odf2-like protein was found to be a component of the centrosome scaffold in somatic cells (Nakagawa *et al*., 2001). The widespread distribution of an Odf2-like protein as a centrosome scaffold component, together with the presence of K5 in the centrosome region of pachytene spermatocytes (Tres *et al*., 1996), and in the acroplaxome (this article) are a demonstration that keratins are used throughout spermatogenesis. Together, these observations strengthen the view that classical keratins (initially identified in the epidermis) and Odf proteins (initially ascribed as sperm-specific proteins) can coex-

ist in the sperm tail to provide structural and mechanical support for stabilizing long flagella while minimizing the risk of kinking or breaking.

The second aspect of the discussion relates to the mechanism of assembly of the acroplaxome and its potential function during spermiogenesis. Concerning the assembly of the acroplaxome, F-actin precedes the appearance of K5 (Figure 7), thus suggesting that it may provide a template for its association with keratin filaments, an event known to occur in vitro (Weber and Bement, 2002). Because the diameter of the acroplaxome increases in parallel with the corresponding spreading of the acrosome over the elongating spermatid nucleus (Figure 7), it is conceivable that this process may occur at the expense of actin polymerization. F-Actin is present in the subacrosomal space during most of spermiogenesis before depolymerizing to G-actin in late spermatids and sperm (reviewed by Vogl, 1989).

A significant question is whether F-actin in the acroplaxome can provide a binding scaffold for motor proteins and contain actin regulatory proteins. The motor protein myosin-Va is present in the acroplaxome (our unpublished observation), and there are precedents for actin regulatory proteins. It is known that binding of the actin-depolymerizing factor cofilin to actin promotes the transition of polymeric F-actin into oligomeric or monomeric G-actin (reviewed in Ayscough, 1998). Phosphorylation of cofilin by LIMK (LIM kinase) prevents cofilin binding and depolymerization of actin, leading to the accumulation of filamentous actin. In this respect, the testicular isoform of LIMK2 is associated with spermatids and targeted *Limk2* gene disruption affects the progression of spermatogenesis (Takahashi *et al*., 2002). Furthermore, a number of actin-binding proteins have been reported at the acrosomal region (for example, actin-capping proteins, Hurst *et al*., 1998; calicin, Lécuyer *et al*., 2000; profilin-3, Braun *et al*., 2002; Arc, Maier *et al*., 2003). A variant of Wiskott-Aldrich syndrome protein-interacting src homology 3 protein (designated WISH) was exclusively found in testis (Fukuoka *et al*., 2001). WISH strongly enhances Wiskott-Aldrich syndrome protein-induced actin-related protein 2/3 (Arp2/3) complex activation, resulting in rapid actin nucleation and polymerization. Given the existence of a number of testis-specific actin binding proteins, an analysis of their role in the regulation of actin assembly and disassembly in the acroplaxome would contribute greatly to advance an understanding of the mechanistic complexity of this structure. An experimental approach to addressing these questions is to sequester actin monomers resulting in rapid depolymerization of F-actin. Unfortunately, the physiological consequences of impairing the function of the acroplaxome by disruptors of the actin cytoskeleton (such as latrunculin A) cannot be assessed in cultured spermatids. First, the developmental time of the acrosome-acroplaxome complex is long (days; Clermont *et al*., 1993). Second, actin-disrupting agents can target the supporting Sertoli cells, which are required for spermatogenic cell viability and differentiation in vivo and in vitro (Kierszenbaum, 1994). Because of these reasons, mouse mutants provide at present a more feasible approach to determine how the acroplaxome might work.

How can the acroplaxome contribute to spermatid nuclear shaping? It is likely that a stress-resistant acroplaxome can transmit gentle and sustained clutching forces generated by Sertoli cell ectoplasmic F-actin bundles to the elongating spermatid nucleus (Figure 9). The spatial arrangement of stacked F-actin hoops embracing the apical one-third of the spermatid nucleus seems to be kept in place by the actin-linked afadin–nectin complex, which may ensure constant Sertoli-spermatid contact (Ozaki-Kuroda *et al*., 2002). In addition to the force exerted by Sertoli cell F-actin hoops, the perinuclear ring of the manchette can provide an endogenous clutch applied at the caudal two-thirds of the spermatid nucleus. As the manchette descends along the elongating spermatid nucleus, its perinuclear ring gradually reduces its diameter and, in a sleeve-like manner, may apply forces steering the elongation of the spermatid nucleus. In fact, fractionated manchette perinuclear rings of various diameters have been demonstrated (Mochida *et al*., 1998), and a nuclear deforming constriction at the level of the perinuclear ring of azh mutant mice spermatids can be seen (Figure 8B). In summary, we have shown that the F-actin–keratin-containing acroplaxome provides a planar scaffold, which maintains the acrosome at the nuclear anchoring site during nuclear elongation. This study provides a novel model for spermatid nuclear shaping, which can be extended by the analysis of a number of mutant mice in which the development of the acrosome and integrity of the acroplaxome are defective.

## ACKNOWLEDGMENTS

This work was supported by U.S. Public Health Service grant HD37282.

## REFERENCES

Akutsu, H., Tres, L.L., Tateno, H., Yanagimachi, R., and Kierszenbaum, A.L. (2001). Offspring from normal mouse oocytes injected with sperm heads from the *azh/azh* mouse display more severe sperm tail abnormalities than the original mutant. Biol. Reprod. *64*, 249–256.

Ayscough, K.R. (1998). In vivo function of actin-binding proteins. Curr. Opin. Cell Biol. *10*, 102–111.

Braun, A., Aszodi, A., Hellebrand, H., Berna, A., Fassler, R., and Brandau, O. (2002). Genomic organization of profilin-III and evidence for a transcript expressed exclusively in testis. Gene *283*, 219–225.

Brohmann, H., Pinnecke, S., and Hoyer-Fender, S. (1997). Identification and characterization of new cDNAs encoding outer dense fiber proteins of rat sperm. J. Biol. Chem. *272*, 10327–10332.

Burfeind, P., and Hoyer-Fender, S. (1991). Sequence and developmental expression of a mRNA encoding a putative protein of rat sperm outer dense fibers. Dev. Biol. *148*, 195–204.

Calvin, H.I. and Bedford, J.M. (1971). Formation of disulphide bonds in the nucleus and accessory structures of mammalian spermatozoa during maturation in the epididymis. J. Reprod. Fertil. *13*(suppl), 65–75.

Clermont, Y., Oko, R., and Hermo, L. (1993). Cell biology of mammalian spermiogenesis. In: Cell and Molecular Biology of the Testis, ed. C. Desjardins and L Ewing, New York: Oxford University Press, 332–376.

Fuchs, E. (1996). The cytoskeleton and disease: genetic disorders of intermediate filaments. Annu. Rev. Genet. *3*, 197–231.

Fukuoka, M., Suetsugu, S., Miki, H., Fukami, K., Endo, T., and Takenawa, T. (2001). A novel neural Wiskott-Aldrich syndrome protein (N-WASP) binding protein, WISH, induces Arp2/3 complex activation independent of Cdc42. J. Cell Biol. *152*, 471–482.

Hurst, S., Howes, E.A., Coadwell, J., and Jones, R. (1998). Expression of a testis-specific putative actin-capping protein associated with the developing acrosome during rat spermiogenesis. Mol. Reprod. Dev. *49*, 81–91.

Kang-Decker, N., Mantchev, G.T., Juneja, S.C., McNiven, M.A., and van Deursen, J.M.A. (2001). Lack of acrosome formation in Hrb-deficient mice. Science *294*, 1531–1533.

Kierszenbaum, A.L. (1994). Mammalian spermatogenesis in vivo and in vitro: a partnership of spermatogenic and somatic cell lineages. Endocr. Rev. *15*, 116–134.

Kierszenbaum, A.L. (2002). Intramanchette transport (IMT): managing the making of the spermatid head, centrosome, and tail. Mol. Reprod. Dev. *63*, 1–4.

Kierszenbaum, A.L., Rivkin, E., Fefer-Sadler, S., Mertz, J.R., and Tres, L.L. (1996). Purification, partial characterization, and localization of Sak57, an

acidic intermediate filament keratin present in rat spermatocytes, spermatids, and sperm. Mol. Reprod. Dev. *44*, 382–394.

Lécuyer, C., Dacheux, J-L., Hermand, E., Mzeman, E., Rousseaux, J., and Rousseaux-Prévost, R. (2000). Actin-binding properties and colocalization with actin during spermiogenesis of mammalian sperm calicin. Biol. Reprod. *63*, 1801–1810.

Maier, B., Medrano, S., Sleight, S.B., Visconti, P.E., and Scrable, H. (2003). Developmental association of the synaptic activity-regulated protein Arc with the mouse acrosomal organelle and the sperm tail. Biol. Reprod. *68*, 67–76.

Meistrich, M.L. (1993). Nuclear morphogenesis during spermiogenesis. In: Molecular Biology of the Male Reproductive System, ed. D. de Kretser, New York: Academic Press, 67–97.

Mochida, K., Rivkin, E., Gil, M., and Kierszenbaum, A.L. (2000). Keratin 9 is a component of the perinuclear ring of the manchette of rat spermatids. Dev. Biol. *227*, 510–519.

Mochida, K., Tres, L.L., and Kierszenbaum, A.L. (1998). Isolation of the rat spermatid manchette and its perinuclear ring. Dev. Biol. *200*, 46–56.

Mochida, K., Tres, L.L., and Kierszenbaum, A.L. (1999). Structural and biochemical features of fractionated spermatid manchettes and sperm axonemes of the *azh/azh* mutant mouse. Mol. Reprod. Dev. *52*, 434–444.

Nakagawa, Y., Yamame, Y., Okanoue, T., Tsukita, S., and Trukita, S. (2001). Outer dense fiber 2 is a widespread centrosome scaffold component preferentially associated with mother centrioles: its identification from isolated centrosomes. Mol. Biol. Cell *12*, 1687–1697.

Oko, R. (1988). Comparative analysis of proteins from the fibrous sheath and outer dense fibers of rat spermatozoa. Biol. Reprod. *39*, 69–182.

Olson, G.E., and Sammons, D.W. (1980). Structural chemistry of outer dense fibers of rat sperm. Biol. Reprod. *22*, 319–332.

Ozaki-Kuroda, K., *et al*. (2002). Nectin couples cell-cell adhesion and the actin scaffold at heterotypic testicular junctions. Curr. Biol. *12*, 1145–1150.

Peters, B., Kirfel, J., Büssow, H., Vidal, M., and Magin, T.M. (2001). Complete cytolysis and neonatal lethality in keratin 5 knockout mice reveal its fundamental role in skin integrity and epidermolysis bullosa simplex. Mol. Biol. Cell *12*, 1775–1789.

Petersen, C., Aumuller, G., Bahrami, M., and Hoyer-Fender, S. (2002). Molecular cloning of Odf3 encoding a novel coiled-coil protein of sperm tail outer dense fibers. Mol. Reprod. Dev. *61*, 102–112.

Rivkin, E., Cullinan, E.B., Tres, L.L., and Kierszenbaum, A.L. (1997). A protein associated with the manchette during rat spermiogenesis is encoded by a gene of the TBP-1-like subfamily with highly conserved ATPase and protease domains. Mol. Reprod. Dev. *47*, 77–89.

Russell, L.D., Weber, J.E., and Vogl, A.W. (1986). Characterization of filaments within the subacrosomal space of rat spermatids during spermiogenesis. Tissue Cell *18*, 887–898.

Szász, F., Sirivaidyapong, S., Cheng, F.P., Voorhout, W.F., Marks, A., Colenbrander, B., Solti, L., and Gadella, B.M. (2000). Detection of calcium ionophore induced membrane changes in dog sperm as a simple method to predict the cryopreservability of dog sperm. Mol. Reprod. Dev. *55*, 289–298.

Takahashi, H., Koshimizu, U., Miyazaki, J., and Nakamura, T. (2002). Impaired spermatogenic ability of testicular germ cells in mice deficient in the LIM-kinase 2 gene. Dev. Biol., *241*, 259–272.

Takai, Y., and Nakanishi, H. (2003). Nectin and afadin: novel organizers of intercellular junctions. J. Cell Sci. *116*, 17–27.

Tres, L.L., and Kierszenbaum, A.L. (1996). Sak57, an acidic keratin initially present in the spermatid manchette before becoming a component of paraaxonemal structures of the developing tail. Mol. Reprod. Dev. *44*, 395–407.

Tres, L.L., Rivkin, E., and Kierszenbaum, A.L. (1996). Sak57, an intermediate filament keratin present in intercellular bridges of rat primary spermatocytes. Mol. Reprod. Dev. *45*, 93–105.

van der Hoorn, F.A., Tarnasky, H.A., and Nordeen, S.K. (1990). A new rat gene RT7 is specifically expressed during spermatogenesis. Dev. Biol. *143*, 147–154.

Vera, J.E., Brito, M., Zuvic, T., and Burzio, L.O. (1984). Polypeptide composition of rat sperm outer dense fibers, A simple procedure to isolate the fibrillar complex. J. Biol. Chem. *259*, 5970–5977.

Vogl, A.W. (1989). Distribution and function of organized concentrations of actin filaments in mammalian spermatogenic cells and Sertoli cells. Int. Rev. Cytol., *119*, 1–56.

Weber, K.L., and Bement, W.M. (2002). F-actin serves as a template for cytokeratin organization in cell free extracts. J. Cell Sci. *115*, 1373–1382.

Yao, R., Ito, C., Natsume, Y., Sugitani, Y., Yamanaka. H., Kuretake, S., Yanagida, K., Sato, A., Toshimori, K., and Noda, T. (2002). Lack of acrosome formation in mice lacking Golgi protein, GOPC. Proc. Natl. Acad. Sci. USA *99*, 11211–11216.